

SED, Age and Metallicity of Star Clusters in M33

Jun Ma¹, Xu Zhou¹, Xu Kong², Hong Wu¹, Jiansheng Chen¹, Zhaoji Jiang¹, Jin Zhu¹, and Suijian Xue¹

Received _____; accepted _____

arXiv:astro-ph/0106487v1 27 Jun 2001

¹National Astronomical Observatories, Chinese Academy of Sciences, Beijing, 100012, P. R. China;
majun@vega.bac.pku.edu.cn

²Center for Astrophysics, University of Science and Technology of China, Hefei, 230026, P. R. China

ABSTRACT

In this paper we present CCD spectrophotometry of the star clusters that were detected by Chandar, Bianchi, & Ford in the nearby spiral galaxy M33, using the images obtained with the Beijing Astronomical Observatory 60/90 cm Schmidt Telescope in 13 intermediate-band filters from 3800 to 10000Å. The observations cover the whole area of M33 with a total integration of 32.75 hours from September 23, 1995 to August 28, 2000. This provides a multi-color map of M33 in pixels of $1''.7 \times 1''.7$. By aperture photometry, we obtain the spectral energy distributions (SEDs) of these star clusters. Using theoretical stellar population synthesis models, we also obtain the distributions of age and metallicity of these star clusters. These clusters formed continuously from $\sim 3 \times 10^6 - 10^{10}$ years, and have a large span of metallicity from $Z = 0.0004$ to $Z = 0.05$.

Subject headings: galaxies: individual (M33) – galaxies: evolution – galaxies: star clusters

1. INTRODUCTION

The importance of the study of star clusters is difficult to overstate, especially in Local Group galaxies. Star clusters, which represent, in distinct and luminous “packets”, single age and single abundance points, and encapsulate at least a partial history of the parent galaxy’s evolution, can provide a unique laboratory for studying the ongoing and past star formation in the parent galaxy. Determination of elemental abundances in cluster stars is crucial to our understanding of the chemical evolution and star formation histories of the galaxy. In addition, studies of star cluster populations could help our understanding of the relationships between cluster formation and the physical morphology of the parent galaxy.

M33 is a small Scd Local Group galaxy, about 15 times farther from us than the LMC (distance modulus is 24.64) (Freedman, Wilson, & Madore 1991; Chandar, Bianchi, & Ford 1999a). It is interesting and important because it represents a morphological type intermediate between the largest “early-type” spirals and the dwarf irregulars in the Local Group (Chandar, Bianchi, & Ford 1999a). Our collaboration, the Beijing-Arizona-Taiwan-Connecticut (BATC) Multicolor Sky Survey (Fan et al. 1997; Zheng et al. 1999), already had this spiral galaxy as part of its galaxy calibration program. The BATC program uses the 60/90 cm Schmidt telescope at the Xinglong Station of Beijing Astronomical Observatory, with its focal plane equipped with a 2048×2048 Ford CCD, and has custom designed a set of 15 intermediate-band filters to do spectrophotometry for preselected 1 deg^2 regions of the northern sky with this CCD system.

For M33, a database of star clusters have been yielded from the ground-based work (Hiltner 1960; Kron & Mayall 1960; Christian & Schommer 1982, 1988; Melnick & D’Odorico 1978), and from the *Hubble Space Telescope* (*HST*) images (Chandar, Bianchi, & Ford 1999a). Especially, Chandar, Bianchi, & Ford (1999a) presented the first unbiased, representative sample of star clusters, sampling a variety of environments from outer regions to spiral arms and central regions, and can be used to probe the global properties of M33.

Since the pioneering work of Tinsley (1972) and Searle et al. (1973), evolutionary population synthesis has become a standard technique to study the stellar populations of galaxies. This is a result of the improvement in the theory of the chemical evolution of galaxies, star formation, stellar evolution and atmospheres, and of the development of synthesis algorithms and the availability of various evolutionary synthesis models. A comprehensive compilation of such models was presented by Leitherer et al. (1996) and Kennicutt (1998). More widely used models are those from the Padova and Geneva group (e.g. Schaerer & de Koter 1997; Schaerer & Vacca 1998; Bressan et al. 1996; Chiosi et al. 1998), GISSEL96 (Charlot & Bruzual 1991; Bruzual & Charlot 1993; Bruzual & Charlot 1996), PEGASE (Fioc & Rocca-Volmerange 1997) and STARBURST99 (Leitherer et al. 1999).

In this paper, we present the SEDs of the star clusters that were detected by Chandar, Bianchi, & Ford (1999a) in M33, and study the distributions of age and metallicity of these clusters by using the theoretical

evolutionary population synthesis methods. The multi-color photometry is powerful to provide the accurate SEDs for these stellar clusters.

The outline of the paper is as follows. Details of observations and data reduction are given in section 2. In section 3, we provide a brief description of the stellar population synthesis models of Bruzual & Charlot (1996). The distributions of metallicity and age are given in section 4. The summary and discussion are presented in section 5.

2. SAMPLE OF STAR CLUSTERS, OBSERVATIONS AND DATA REDUCTION

2.1. Sample of Star Clusters

The sample of star clusters in this paper is from Chandar, Bianchi, & Ford (1999a), who used 20 multiband *Hubble Space Telescope* (*HST*) WFPC2 fields to search for star clusters much closer to the nucleus of M33 than previous studies. Since these star clusters populate the variety of environments from the outer regions to spiral arms and central regions, they can be used to probe the global properties of the parent galaxy. At the same time, the accurate positions are presented in Table 2 of Chandar, Bianchi, & Ford (1999a). So, as a first step, we select these star clusters to be studied, and obtain their SEDs by aperture photometry. The distribution of age and metallicity for these star clusters are derived by using the theoretical evolutionary population synthesis methods. Clusters 17, 39, 41 and 42 are not included in our sample because of their low signal-to-noise ratio in the images of some BATC filters.

2.2. CCD Image Observation

The large field multi-color observations of the spiral galaxy M33 were obtained in the BATC photometric system. The telescope used is the 60/90 cm f/3 Schmidt Telescope of Beijing Astronomical Observatory (BAO), located at the Xinglong station. A Ford Aerospace 2048×2048 CCD camera with 15 μm pixel size is mounted at the Schmidt focus of the telescope. The field of view of the CCD is $58' \times 58'$ with a pixel scale of $1''.7$.

The multi-color BATC filter system includes 15 intermediate-band filters, covering the total optical wavelength range from 3000 to 10000Å (see Fan et al. 1996). The filters were specifically designed to avoid contamination from the brightest and most variable night sky emission lines. A full description of the BAO Schmidt telescope, CCD, data-taking system, and definition of the BATC filter systems are detailed elsewhere (Fan et al. 1996; Zheng et al. 1999). The images of M33 covering the whole optical body of M33 were accumulated in 13 intermediate band filters with a total exposure time of about 32.75 hours from September 23, 1995 to August 28, 2000. The CCD images are centered at $\text{RA} = 01^{\text{h}}33^{\text{m}}50^{\text{s}}.58$

and DEC=30°39′08″.4 (J2000). The dome flat-field images were taken by using a diffuse plate in front of the correcting plate of the Schmidt telescope. For flux calibration, the Oke-Gunn primary flux standard stars HD19445, HD84937, BD+262606 and BD+174708 were observed during photometric nights. The parameters of the filters and the statistics of the observations are given in Table 1. Figure 1 is “True-color” estimate of M33 generated by using the BATC03 (4210Å) filter image for blue, BATC07 (5785Å) for green, and BATC10 (7010Å) for red.

2.3. Image Data Reduction

The data were reduced with standard procedures, including bias subtraction and flat-fielding of the CCD images, with an automatic data reduction software named PIPELINE 1 developed for the BATC multi-color sky survey (Fan et al. 1996; Zheng et al. 1999). The flat-fielded images of each color were combined by integer pixel shifting. The cosmic rays and bad pixels were corrected by comparison of multiple images during combination. The images were re-centered and position-calibrated using the *HST* Guide Star Catalog. The absolute flux of intermediate-band filter images was calibrated using observations of standard stars. Fluxes as observed through the BATC filters for the Oke-Gunn stars were derived by convolving the SEDs of these stars with the measured BATC filter transmission functions (Fan et al. 1996). *Column 6* in Table 1 gives the zero point error, in magnitude, for the standard stars in each filter. The formal errors we obtain for these stars in the 13 BATC filters are $\lesssim 0.02$ mag. This indicates that we can define the standard BATC system to an accuracy of $\lesssim 0.02$ mag.

2.4. Integrated Photometry

For each star cluster, aperture photometry was used to obtain magnitudes. For avoiding contamination from nearby objects, a smaller aperture of 6″.8, which corresponds to a diameter of 4 pixels in Ford CCDs, was adopted. Considering the large seeing of the Xinglong station, aperture corrections were computed using isolated stars. Since these star clusters sample a variety of environments from outer regions to spiral arms and central regions, background subtraction is difficult. We determined the background in annulus of from 2 to 5 pixels from each star cluster. In this annulus, we fitted each row of the image by linear

Fig. 1.— “True-color” estimate of M33 generated by using the BATC03 (4210Å) filter image for blue, BATC07 (5785Å) for green, and BATC10 (7010Å) for red; the image is balanced by making the background old population orange and hot stars blue. The center (origin) of the image is located at RA = 01^h33^m50^s.58 DEC=30°39′08″.4 (J2000.0). North is up and east is to the left.

median fitting to obtain a surface. Then, we repeat this process in the column direction of the surface that is obtained in the row of fitting. After this fit, we reject points higher and lower than 30 percent of the mean background. Finally, we obtained the final smoothed surface of background. Using this surface of background, we made the background subtraction for each cluster. The spectral energy distributions (SEDs) for the 56 star clusters were obtained. Table 2 contains the following information: *Column 1* is cluster number which is taken from Chandar, Bianchi, & Ford (1999a). *Column 2* to *Column 14* show the magnitudes of different bands. Second line of each star cluster is the uncertainties of magnitude of corresponding band. The uncertainties for each filter take into account the error from the object count rate, sky variance, and instrument gain.

2.5. Comparison with Previous Photometry

Using the Landolt standards, Zhou et al. (2001) presented the relationships between the BATC intermediate-band system and UBVRI broadband system by the catalogs of Landolt (1983, 1992) and Galadí-Enríquez et al. (2000). We show the coefficients of the fits in equations 1 and 2.

$$m_B = m_{04} + (0.2218 \pm 0.033) \times (m_{03} - m_{05}) + 0.0741 \pm 0.033, \quad (1)$$

$$m_V = m_{07} + (0.3233 \pm 0.019) \times (m_{06} - m_{08}) + 0.0590 \pm 0.010. \quad (2)$$

Using equations 1 and 2, we transformed the magnitudes of the star clusters in BATC03, BATC04 and BATC05 bands to ones in B band, and in BATC06, BATC07 and BATC08 bands to ones in V band. For clusters 1, 7, 37, 40 and 43, we change m_{05} to m_{04} because of the strong emission or absorption lines in BATC05 band. Figure 2 plots the comparison of V (BATC) and $(B-V)$ (BATC) photometry with previously published measurements (Chandar, Bianchi, & Ford 1999a). Table 3 also shows this comparison. The mean V magnitude and color differences (this paper – the paper (of Chandar, Bianchi, & Ford 1999a)) are $\langle \Delta V \rangle = -0.009 \pm 0.025$ and $\langle \Delta(B - V) \rangle = -0.179 \pm 0.039$, respectively. The uncertainties in B (BATC) and V (BATC) have been added linearly, i.e. $\sigma_B = \sigma_{04} + 0.2218 \times (\sigma_{03} + \sigma_{05})$, and $\sigma_B = \sigma_{07} + 0.3233 \times (\sigma_{06} + \sigma_{08})$, to reflect the error in the three filter measurements. For the colors, we also added the errors linearly, i.e. $\sigma_{(B-V)} = \sigma_B + \sigma_V$.

3. DATABASES OF SIMPLE STELLAR POPULATIONS

A simple stellar population (SSP) is defined as a single generation of coeval stars with fixed parameters such as metallicity, initial mass function, etc. (Buzzoni 1997). SSPs are the basic building blocks of synthetic spectra of galaxies that can be used to infer the formation and subsequent evolution of the parent galaxies (Jablonka et al. 1996). They are modeled by a collection of stellar evolutionary tracks with

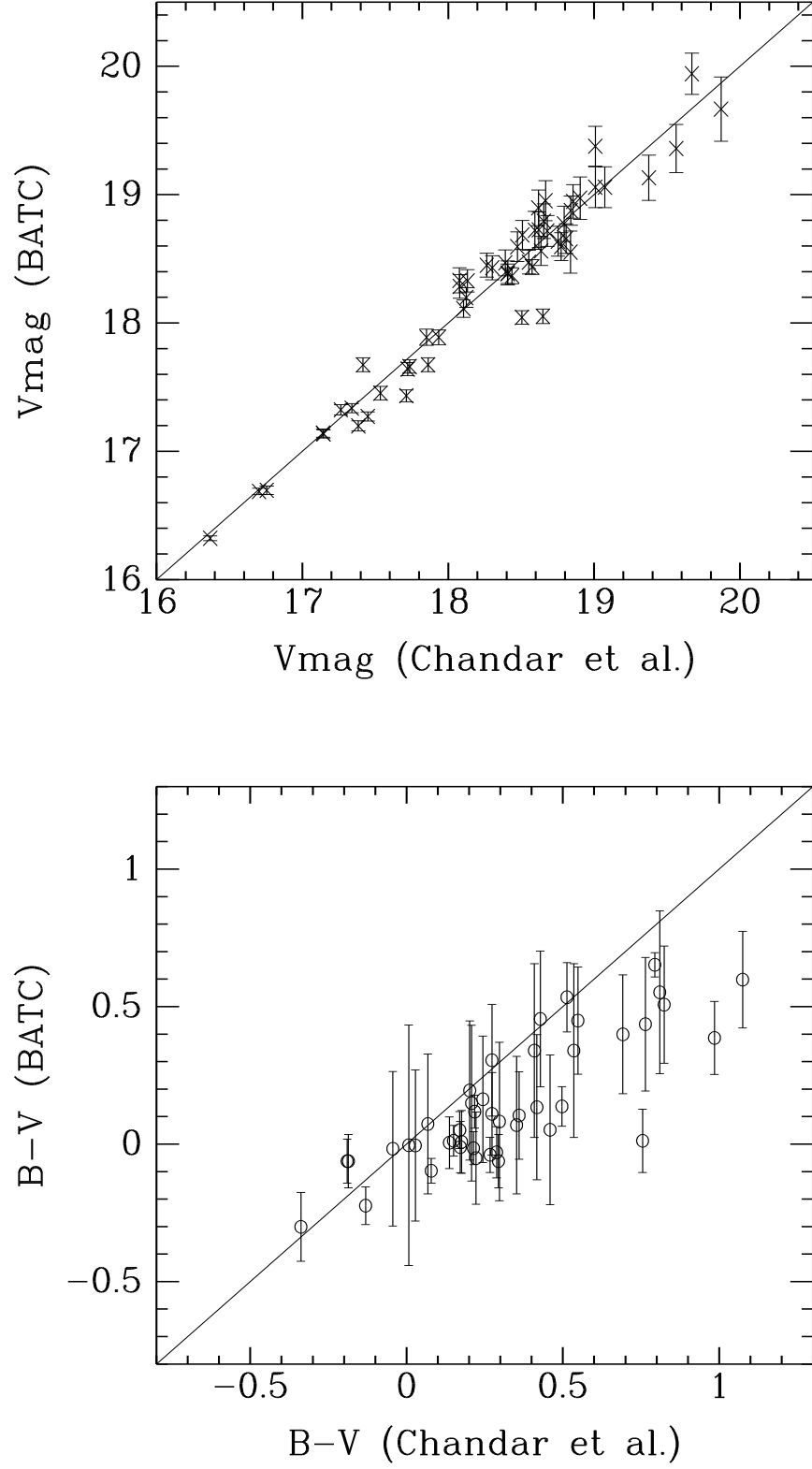


Fig. 2.— Comparison of Cluster Photometry with Previous Measurements

different masses and initial chemical compositions, supplemented with a library of stellar spectra for stars at different evolutionary stages in evolution synthesis models. In order to study the integrated properties of star clusters in M33, as the first step, we use the SSPs of Galaxy Isochrone Synthesis Spectra Evolution Library (Bruzual & Charlot 1996 hereafter GSSP) because they are simple and reasonably well understood.

3.1. Spectral Energy Distribution of GSSPs

The Bruzual & Charlot (1996) study has extended the Bruzual & Charlot (1993) evolutionary population synthesis models. The updated version provides the evolution of the spectrophotometric properties for a wide range of stellar metallicity. They are based on the stellar evolution tracks computed by Bressan et al. (1993), Fagotto et al. (1994), and by Girardi et al. (1996), who use the radiative opacities of Iglesias et al. (1992). This library includes tracks for stars with metallicities $Z = 0.0004, 0.004, 0.008, 0.02, 0.05$, and 0.1 , with the helium abundance given by $Y = 2.5Z + 0.23$ (The reference solar metallicity is $Z_{\odot} = 0.02$). The stellar spectra library is from Lejeune et al. (1997, 1998) for all the metallicities listed above, which in turn consists of Kurucz (1995) spectra for the hotter stars (O-K), Bessell et al. (1991) and Fluks et al. (1994) spectra for M giants, and Allard & Hauschildt (1995) spectra for M dwarfs. GSSP models assume an initial Salpeter (1955) mass function $\Phi(M) = A \times M^{-\alpha}$ with $\alpha = 2.35$ and normalization constant $A = 1$, and a lower cutoff $M_l = 0.1M_{\odot}$ and an upper cutoff $M_u = 125M_{\odot}$ (Sawicki & Yee 1998).

3.2. Integrated Colors of GSSPs

Kong et al. (2000) have obtained the age, metallicity, and interstellar-medium reddening distribution for M81. They found the best match between the intrinsic colors and the predictions of GSSP for each cell of M81. To determine the distributions of age and metallicity of the star clusters in M33, we follow the method of Kong et al. (2000). Since the observational data are integrated luminosity, we need to convolve the SED of GSSP with BATC filter profiles to obtain the optical and near-infrared integrated luminosity for comparisons (Kong et al. 2000). The integrated luminosity $L_{\lambda_i}(t, Z)$ of the i th BATC filter can be calculated with

$$L_{\lambda_i}(t, Z) = \frac{\int F_{\lambda}(t, Z) \varphi_i(\lambda) d\lambda}{\int \varphi_i(\lambda) d\lambda}, \quad (3)$$

where $F_{\lambda}(t, Z)$ is the spectral energy distribution of the GSSP of metallicity Z at age t , $\varphi_i(\lambda)$ is the response functions of the i th filter of the BATC filter system ($i = 3, 4, \dots, 15$), respectively.

The absolute luminosity can be obtained if we know the distance to M33 and the extinction along the line of sight. However, we do not know these parameters exactly. So, we should work with the colors because of their independence of the distance. We calculate the integrated colors of a GSSP relative to the BATC filter BATC08 ($\lambda = 6075\text{\AA}$):

$$C_{\lambda_i}(t, Z) = L_{\lambda_i}(t, Z)/L_{6075}(t, Z). \quad (4)$$

As a result, we obtain intermediate-band colors for 6 metallicities from $Z = 0.0004$ to $Z = 0.1$.

4. REDDENING CORRECTION AND DISTRIBUTIONS OF METALLICITY, AGE

In general, the SED of a stellar system depends on age, metallicity and reddening along the line of sight. The effects of age, metallicity and reddening are difficult to separate (e.g. Calzetti 1997; Origlia et al. 1999; Vazdekis et al. 1997). Older age, higher metallicity or larger reddening all lead to redder SEDs of stellar systems in the optical (Mollà et al. 1997; Bressan et al. 1996). In order to obtain intrinsic colors for these star clusters, we must correct for reddening.

4.1. Reddening Correction

In order to obtain intrinsic colors of 56 clusters and hence accurate ages, the photometric measurements must be dereddened. The observed colors are affected by two sources of reddening: (1) the foreground extinction in our Milky Way and (2) internal reddening due to varying optical paths through the disk of the parent galaxy. McClure & Racine (1969) has measured the foreground color excess, 0.03 ± 0.02 for M33. As Chandar, Bianchi, & Ford (1999b) did, we also adopted this value. For internal reddening of the star clusters, we adopted the values in the third column of Table 3 of Chandar, Bianchi, & Ford (1999b). Besides, we adopted the extinction curve presented by Zombeck (1990). An extinction correction $A_\lambda = R_\lambda E(B - V)$ was applied, here R_λ is obtained by interpolating using the data of Zombeck (1990).

4.2. Age and Metallicity Distribution

Since we model the stellar populations of the star clusters by SSPs, the intrinsic colors for each star cluster are determined by two parameters: age, and metallicity. In this section, we will determine these two parameters for these star clusters simultaneously by a least square method. The best fit age and metallicity are found by minimizing the difference between the intrinsic and integrated colors of GSSP:

$$R^2(n, t, Z) = \sum_{i=3}^{15} [C_{\lambda_i}^{\text{intr}}(n) - C_{\lambda_i}^{\text{ssp}}(t, Z)]^2, \quad (5)$$

where $C_{\lambda_i}^{\text{ssp}}(t, Z)$ represents the integrated color in the i th filter of a SSP with age t and metallicity Z , and $C_{\lambda_i}^{\text{intr}}(n)$ is the intrinsic integrated color for n th star cluster. From Chandar, Bianchi, & Ford (1999b), the distribution of metallicity of these star clusters is from ~ 0.0002 to 0.03 . So, we only select the modles of

three metallicities, 0.0004, 0.004 and 0.02 of GSSP.

Figure 3 shows the map of the best fit of the integrated color of a SSP with the intrinsic integrated color for 56 star clusters, and Table 4 presents the ages and metallicities of these 56 star clusters. In Figure 3, the thick line represents the integrated color of a SSP of GSSP, and filled circle represents the intrinsic integrated color of a star cluster. From this figure, we also see that clusters 1, 7, 8, 40 and 43 have strong emission lines. For cluster 2, since the fitting is not good in the above models of the three metallicities of GSSP (showing by dashed line in Figure 3), we again select a model of a higher metallicity, 0.05 (showing by the thick line in Figure 3). We find that this model of metallicity of 0.05 can be fitted much better for cluster 2.

Figure 4 presents a histogram of cluster ages. The results show that, in general, M33 clusters have been forming continuously, with ages of $\sim 3 \times 10^6 - 10^{10}$ years. This conclusion is consistent with that found by Chandar, Bianchi, & Fort (1999b). There exist three groups of clusters that formed with three metallicities, $Z = 0.02, 0.004$, and 0.0004 . With different metallicities, the distribution of cluster ages is a little different, too. With $Z = 0.02$ metallicity, the ages of clusters are younger than $\sim 4 \times 10^9$ years. With $Z = 0.004$, the clusters formed from $\sim 3 \times 10^6 - 10^{10}$ years. With $Z = 0.0004$, the clusters formed from $\sim 10^8 - 10^{10}$ years except of cluster 8. In this model, there are 15 young clusters ($< 10^9$ years). Except of cluster 26, which is near the center of the host galaxy ($\sim 1'.7$ far from the center), the other clusters are farther than $4'.0$ from the center (nearer than $12'.6$). This population of young, metal-poor clusters appears to not be in the outskirts of the parent galaxy. Clusters 11 and 57 have derived ages consistent with that of the globular clusters of the Milky Way, $\sim 1.5 \times 10^{10}$ years. This result is also consistent with that found by Chandar, Bianchi, & Fort (1999b), who presented clusters 28 and 29 to be as old as $\sim 1.5 \times 10^{10}$ years. From our small sample clusters, we cannot see any evidence for an abundance gradient. The main reason may be that, integrated colors of star clusters depend mostly on age, with a secondary dependence on chemical composition. So, we can estimate ages of clusters, but cannot determine metallicities of clusters exactly. As Chandar, Bianchi, & Ford (1999b, 1999c) did, we also estimated the ages of our sample clusters by comparing the photometry of each object with models for different values of metallicity. Although we presented the metallicity of each cluster in Table 4, we only mean that, in this model of metallicity, the intrinsic integrated color of each cluster can do the best fit with the integrated color of a SSP.

Kong et al. (2000) found a relation between flux ratio of $I_{8510} \equiv L_{8510}/L_{9170}$ and metallicity for stellar populations older than 1 Gyr. Using this relation, we can provide an independent estimate of metallicity for our older clusters without an assumption of reddening. But, this method can be only used when the signal-to-noise ratio is high enough. In our sample clusters of M33, the signal-to-noise ratios are not high enough because of the strong background (These clusters distribute mainly in the spiral arms and central regions.). So, the metallicities of the old clusters derived via the technique of Kong et al. (2000) are also

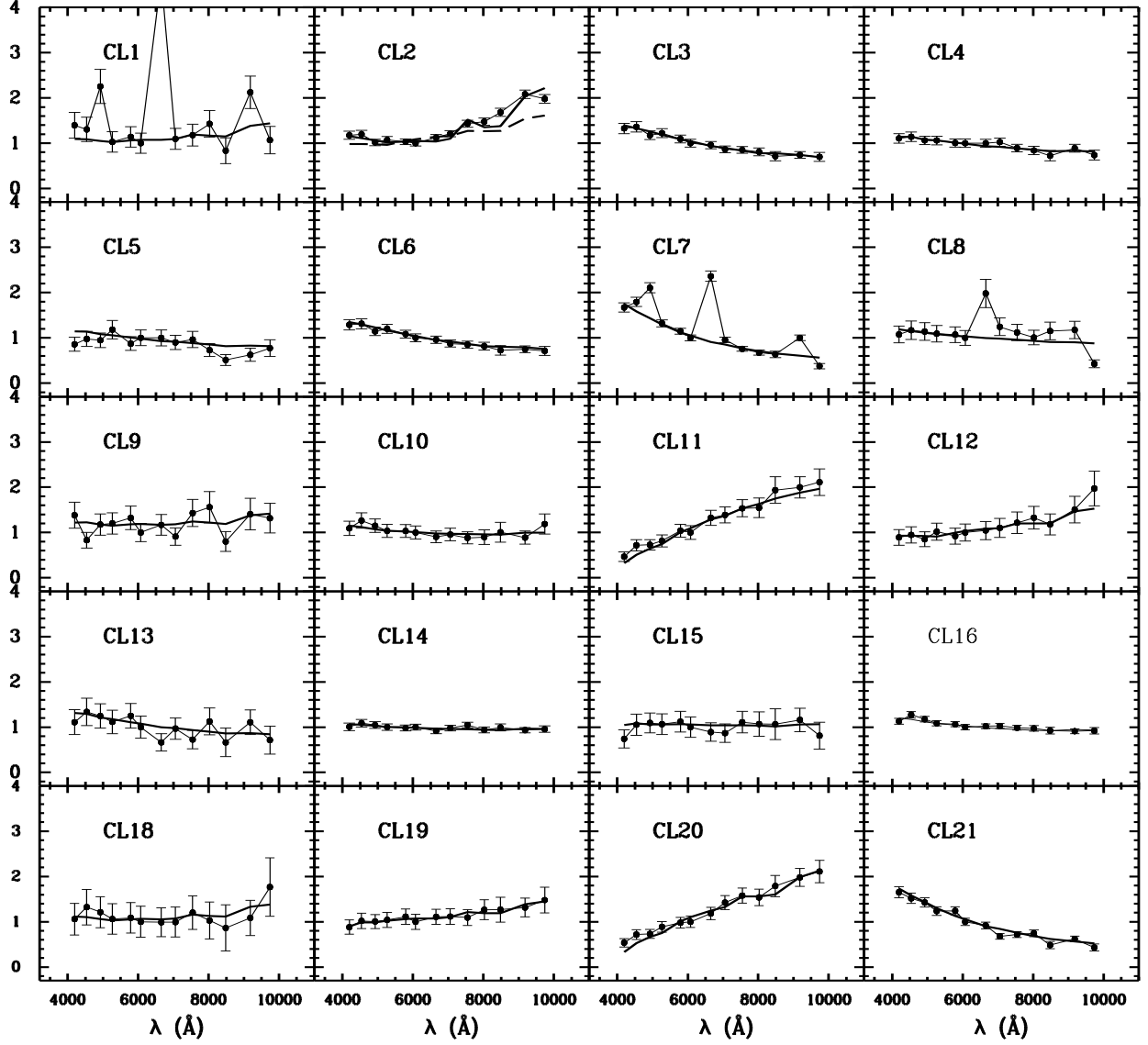


Fig. 3.— Map of the best fit of the integrated color of a SSP with intrinsic integrated color for 56 star clusters. Thick line represents the integrated color of a SSP, and filled circle represents the intrinsic integrated color of a star cluster.

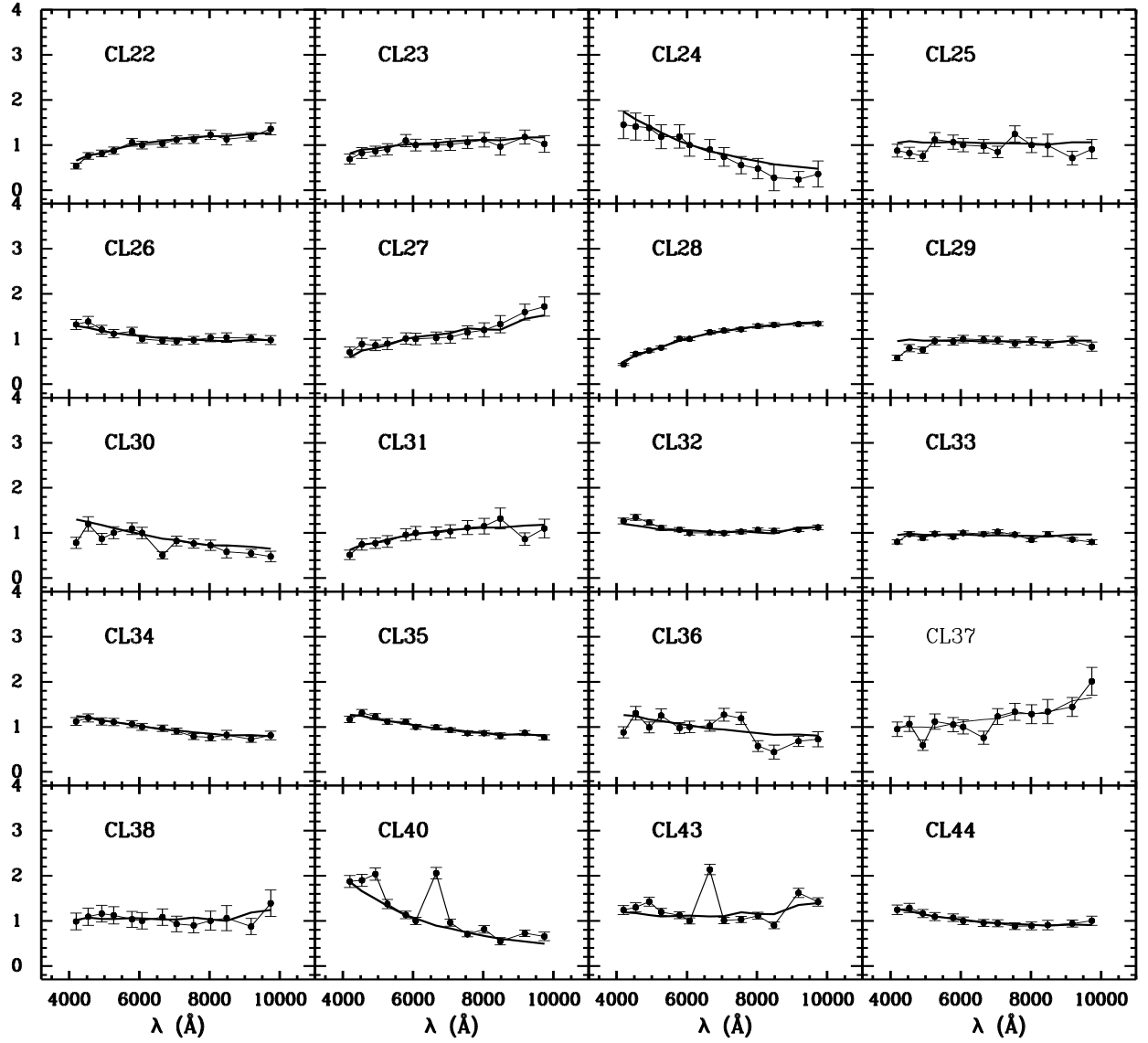


Fig. 3.— Continued

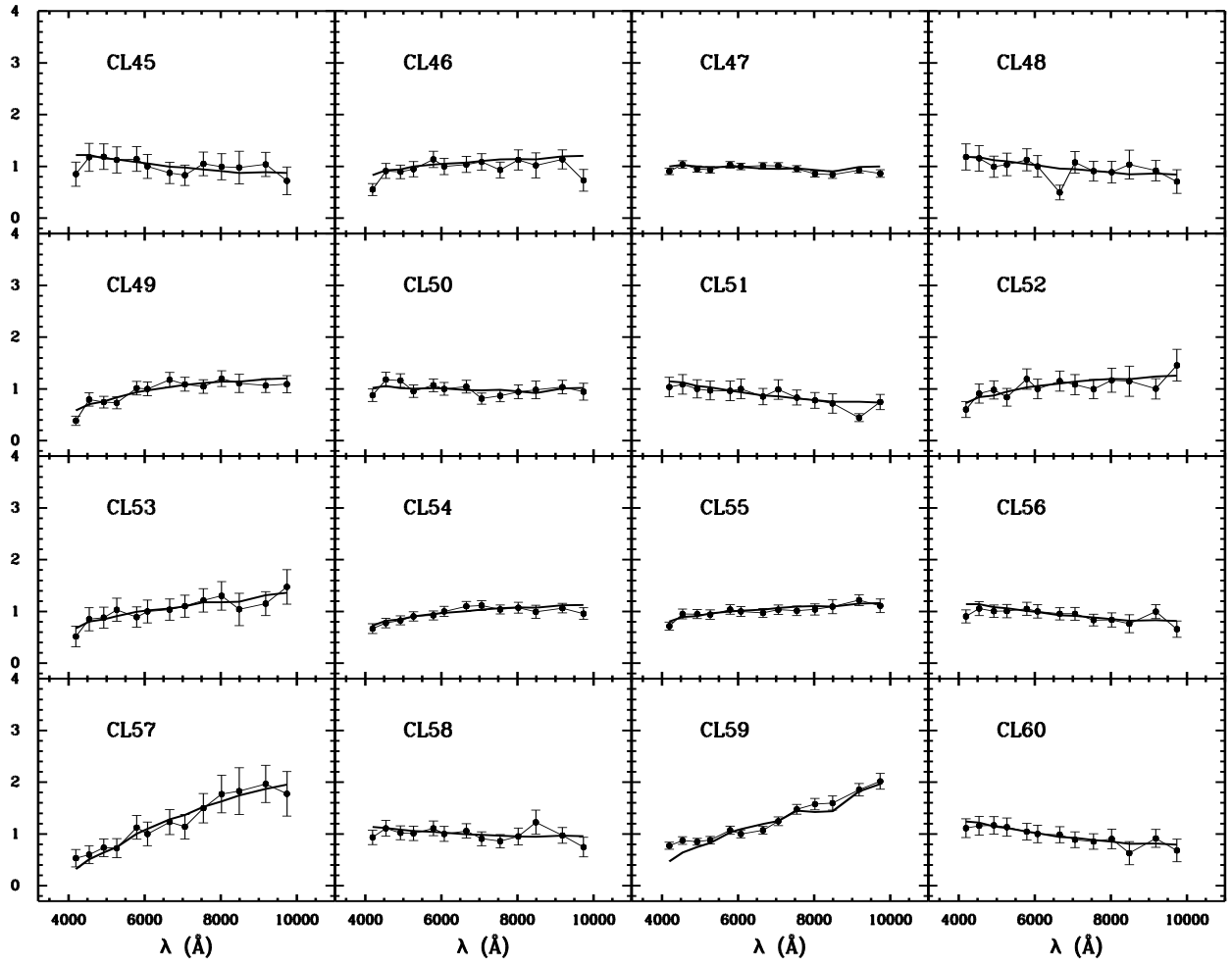


Fig. 3.— Continued

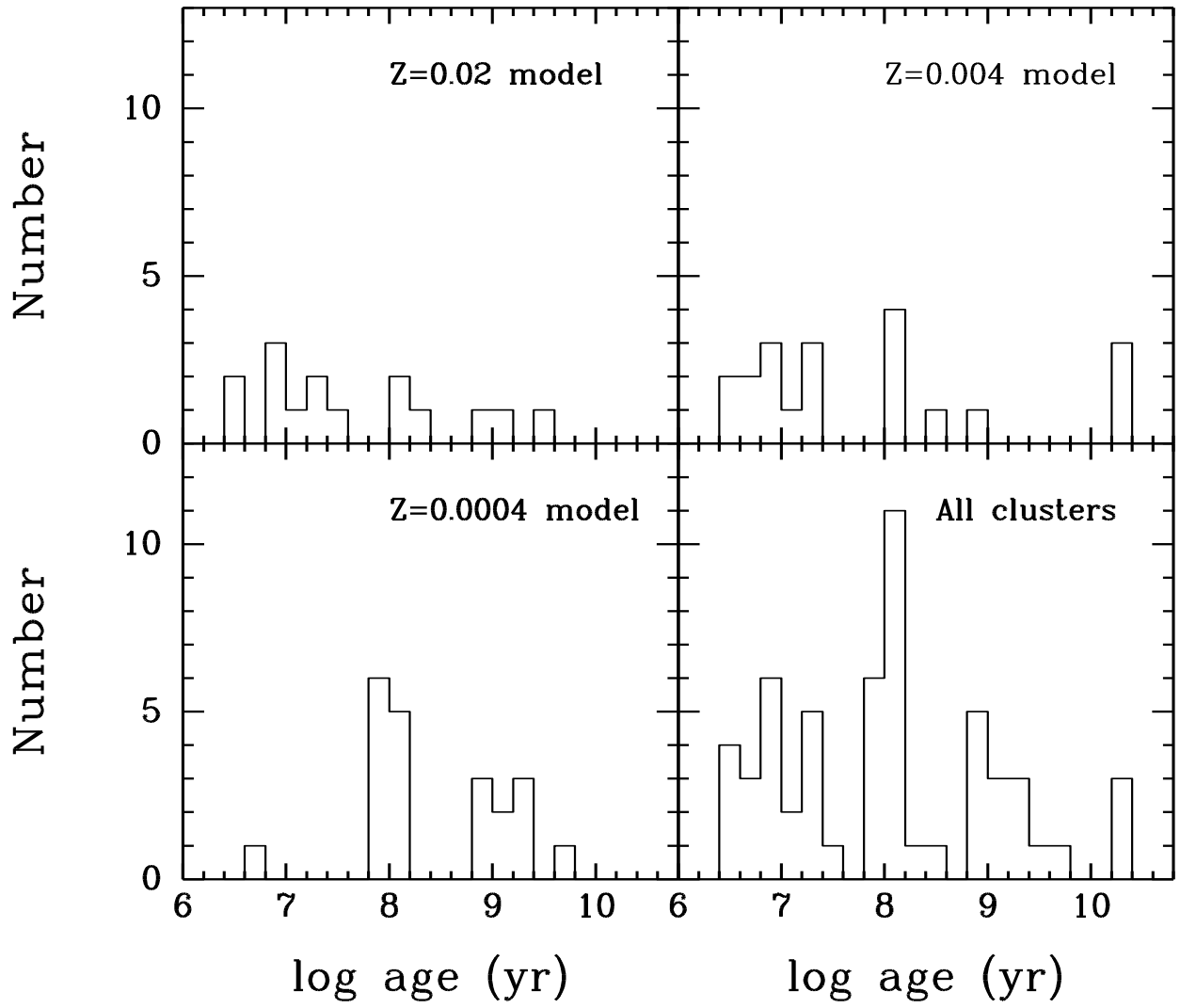


Fig. 4.— Histogram of M33 cluster ages

somewhat uncertain. In our paper, there are 10 clusters, the ages of which are 1 Gyr or older than 1 Gyr. We calculated their metallicities using the method of Kong et al. (2000) except of clusters 31, 52 and 57, since the magnitude uncertainties of these three clusters are too large. Then we obtained their reddenings and ages. The results are listed in Table 5. From this table and Table 4, we can see that the metallicities of clusters 11 and 54 are not consistent by two methods. We also see that, except of clusters 20 and 59, the cluster ages derived by two methods, are consistent. The values of reddening obtained by the method of Kong et al. (2000), are not consistent with ones of Chandar, Bianchi, & Fort (1999b) except of clusters 20, 22 and 28. But, as we know the reddening is difficult to estimate.

5. SUMMARY AND DISCUSSION

In this paper, we have, for the first time, obtained the SEDs of 56 star clusters of M33 in 13 intermediate colors with the BAO 60/90 cm Schmidt telescope. Below, we summarize our main conclusions.

1. Using the images obtained with the Beijing Astronomical Observatory 60/90 cm Schmidt Telescope in 13 intermediate-band filters from 3800 to 10000 Å, we obtained the spectral energy distributions (SEDs) of the star clusters that were detected by Chandar, Bianchi, & Ford (1999a).
2. Using theoretical stellar population synthesis models, we obtained the distributions of age and metallicity of these star clusters. These clusters formed continuously from $\sim 3 \times 10^6 - 10^{10}$ years, and have a large span of metallicity from $Z = 0.0004$ to $Z = 0.05$.

With ~ 10 Å resolution spectrophotometry ($\lambda\lambda 3700 - 5500$ Å), Christian & Schommer (1983) presented that M33 star clusters have a range of ages ($\sim 10^7 - 10^{10}$ years). Using the integrated *UBV* photometry and IUE $\lambda\lambda 1200 - 3000$ Å spectra, Ciani, D’Odorico, & Benvenuti (1984) studied the minuscule “bulge” population of M33 and found that, a multigeneration model, where a young component (age $\sim 10^7$ years) and an old, metal-poor one (age $\sim 5 \times 10^9$ years) are superposed, gives the best fit to the observed data. Schmidt, Bica, & Alloin (1990) applied a population synthesis method which uses a star cluster spectral library and a grid of the star cluster spectral properties as a function of age and metallicity (Bica & Alloin 1986a, b; 1987), to the blueish nucleus of M33, and gave an age of less than 5×10^8 years for the dominant blue bulge population. From the histogram of ages in this paper, we can see that some old clusters in our sample appear to be coeval with the old population of the bulge. Chandar, Bianchi, & Ford (1999b, 1999c) also estimated ages for the star clusters of this paper by comparing the *UBV* and far-UV photometric measurements (Chandar, Bianchi, & Ford 1999a, 1999c) to integrated colors from theoretical models by Bertelli et al. (1994), and found that these clusters formed continuously from $\sim 4 \times 10^6 - 10^{10}$ years. Our results are consistent with the conclusions of Chandar, Bianchi, & Ford (1999b, 1999c).

To disentangle age, metallicity and reddening in SSPs, we adopted the $E(B - V)$ values presented

in Chandar, Bianchi, & Ford (1999b). These values may be somewhat uncertain. In order to see clearly how the uncertainties of $E(B - V)$ affect the derived age and metallicity, we adopt an uncertainty of 0.03 magnitudes of the $E(B - V)$ values given in Chandar, Bianchi, & Ford (1999b). The results appear that an uncertainty of 0.03 magnitudes in $E(B - V)$ hardly affects the derived ages and metallicities on the average, but have a somewhat larger affect on the older clusters.

We would like to thank the anonymous referee for his/her insightful comments and suggestions that improved this paper. We are grateful to the Padova group for providing us with a set of theoretical isochrones and SSPs. We also thank G. Bruzual and S. Charlot for sending us their latest calculations of SSPs and for explanations of their code. The BATC Survey is supported by the Chinese Academy of Sciences, the Chinese National Natural Science Foundation and the Chinese State Committee of Sciences and Technology. The project is also supported in part by the National Science Foundation (grant INT 93-01805) and by Arizona State University, the University of Arizona and Western Connecticut State University.

REFERENCES

- Allard, F., & Hauschildt, P. H. 1995, *ApJ*, 445, 433
- Bessell, M. S., Brett, J. M., Scholz, M., & Wood, P. R. 1991, *A&AS*, 89, 335
- Bertelli, G., Bressan, A., Chiosi, C., Fagotto, F., & Nasi, E. 1994, *A&AS*, 106, 275
- Bica, E., & Alloin, D. 1986a, *A&A*, 162, 21
- Bica, E., & Alloin, D. 1986b, *A&AS*, 66, 171
- Bica, E., & Alloin, D. 1987, *A&A*, 186, 49
- Bressan, A., et al. 1993, *A&AS*, 100, 647
- Bressan, A., Chiosi, C., & Tantalo, R. 1996, *A&A*, 311, 425
- Bruzual, G., & Charlot, S. 1993, *ApJ*, 405, 538
- Bruzual, G., & Charlot, S. 1996, Documentation for GISSEL96 Spectral Synthesis Code.
- Buzzoni, A. 1997, in *IAU Symp. 183, Cosmological Parameters and Evolution of the Universe*, ed. K. Sato, 18
- Calzetti, D. 1997, *AJ*, 113, 162
- Chandar, R., Bianchi, L., & Ford, H. C. 1999a, *ApJS*, 122, 431
- Chandar, R., Bianchi, L., & Ford, H. C. 1999b, *ApJ*, 517, 668
- Chandar, R., Bianchi, L., Ford, H. C., & Salasnich, B. 1999c, *PASP*, 111, 794
- Charlot, S., & Bruzual, G. 1991, *ApJ*, 367, 126
- Charlot, S., Worthey, G., & Bressan, A. 1996, *ApJ*, 457, 625
- Chiosi, C., Bressan, A., Portinari, L., & Tantalo, R. 1998, *A&A*, 339, 355
- Christian, C. A., & Schommer, R. A. 1982, *ApJS*, 49, 405
- Christian, C. A., & Schommer, R. A. 1983, *ApJ*, 275, 92
- Christian, C. A., & Schommer, R. A. 1988, *AJ*, 95, 704
- Ciani, A., D’Odorico, S., & Benvenuti, P. 1984, *A&A*, 137, 223

- Fagotto, F., Bressan, A., Bertelli, G., & Chiosi, C. 1994, *A&AS*, 105, 39
- Fan, X.-H., et al. 1996, *AJ*, 112, 628
- Fioc, M., & Rocca-Volmerange, B. 1997, *A&A*, 326,950
- Fluks, M. A., Plez, B., Thé, P. S., de Winter, D., Westerlund, B. E., & Steenman, H. C. 1994, *A&AS*, 105, 311
- Freedman, W. L., Wilson, C. D., & Madore, B. F. 1991, *ApJ*, 372, 455
- Galadí-Enríquez, D., Trullols, E., & Jordi, C. 2000, *A&AS*, 146, 169
- Girardi, L., Bressan, A., Chiosi, C., Bertelli, G., & Nasi, E. 1996, *A&AS*, 117, 113
- Hiltner, W. A. 1960, *ApJ*, 131, 163
- Iglesias, C. A., Rogers, F. J., & Wilson, B. G. 1992, *ApJ*, 397, 717
- Jablonka, P., Bica, E., Pelat, D., & Alloin, D. 1996, *A&A*, 307, 385
- Kennicutt, R. C. 1998, *A&A Rev.*, 36, 189
- Kong, X. et al. 2000, *AJ*, 119, 2745
- Kron, G. E., & Mayall, N. U. 1960, *AJ*, 65, 581
- Kurucz, R. L. 1995 (private communication)
- Landolt, A. U. 1983, *AJ*, 88, 439
- Landolt, A. U. 1992, *AJ*, 104, 340
- Leitherer, C., et al. 1996, *PASP*, 108, 996
- Leitherer, C., et al. 1999, *ApJS*, 123, 3
- Lejeune, Th., Cuisinier, F., & Buser, R. 1997, *A&AS*, 125, 229
- Lejeune, Th., Cuisinier, F., & Buser, R. 1998, *A&AS*, 130, 65
- McClure, R. D., & Racine, R. 1969, *AJ*, 74, 1000
- Melnick, J., & D’Odorico, S. 1978, *A&AS*, 34, 249
- Mollà, M., Ferrini, F., & Diaz, A. I. 1997, *ApJ*, 475, 519

- Origlia, L., Goldader, J. D., Leitherer, C., & Schaerer, D., & Oliva, E. 1999, *ApJ*, 514, 96
- Salpeter, E. E. 1955, *ApJ*, 121, 161
- Sarajedini, A. A., Geisler, D., Harding, P., & Schommer, R. 1998, *ApJ*, 508, L37
- Sawicki, M., & Yee, H. K. C. 1998, *AJ*, 115, 1329
- Schaerer, D., & de Koter, A. 1997, *A&A*, 322, 598
- Schaerer, D., & Vacca, W. D. 1998, *ApJ*, 497, 618
- Schmidt, A. A., Bica, E., & Alloin, D. 1990, *MNRAS*, 243, 620
- Searle, L., Sargent, W. L. W., & Bagnuolo, W. G. 1973, *ApJ*, 179, 427
- Tinsley, B. M. 1972, *A&A*, 20, 382
- Vazdekis, A., Peletier, R. F., Beckman, J. E., & Casuso, E. 1997, *ApJS*, 111, 203
- Zheng, Z. Y., et al. 1999, *AJ*, 117, 2757
- Zhou, X., et al. 2001, in preparation
- Zombeck, M. V. 1990, *Handbook of Space Astronomy and Astrophysics* (2nd. ed; Cambridge: Cambridge Univ. Press) p. 104

Table 1: Parameters of the BATC filters and statistics of observations

No.	Name	cw ^a (Å)	Exp. (hr)	N.img ^b	rms ^c
1	BATC03	4210	00:55	04	0.024
2	BATC04	4546	01:05	04	0.023
3	BATC05	4872	03:55	19	0.017
4	BATC06	5250	03:19	15	0.006
5	BATC07	5785	04:38	17	0.011
6	BATC08	6075	01:26	08	0.016
7	BATC09	6710	01:09	08	0.006
8	BATC10	7010	01:41	08	0.005
9	BATC11	7530	02:07	10	0.017
10	BATC12	8000	03:00	11	0.003
11	BATC13	8510	03:15	11	0.005
12	BATC14	9170	01:15	05	0.011
13	BATC15	9720	05:00	26	0.009

^aCentral wavelength for each BATC filter

^bImage numbers for each BATC filter

^cZero point error, in magnitude, for each filter as obtained from the standard stars

Table 2: SEDs of 56 Star Clusters

No.	03	04	05	06	07	08	09	10	11	12	13	14
(1)	(2)	(3)	(4)	(5)	(6)	(7)	(8)	(9)	(10)	(11)	(12)	(13)
1..	18.617	18.650	18.017	18.819	18.647	18.769	17.066	18.620	18.520	18.282	18.835	17.801
	0.073	0.078	0.039	0.100	0.081	0.107	0.024	0.098	0.095	0.098	0.245	0.060
2..	16.684	16.623	16.760	16.653	16.635	16.648	16.492	16.392	16.189	16.125	15.954	15.702
	0.019	0.019	0.019	0.021	0.018	0.022	0.019	0.018	0.017	0.017	0.020	0.012
3..	17.611	17.552	17.672	17.589	17.660	17.727	17.753	17.836	17.841	17.868	17.976	17.923
	0.030	0.029	0.028	0.031	0.032	0.039	0.038	0.044	0.046	0.064	0.108	0.062
4..	17.879	17.816	17.853	17.815	17.824	17.799	17.782	17.723	17.864	17.898	18.029	17.795
	0.037	0.036	0.032	0.038	0.037	0.042	0.039	0.040	0.048	0.067	0.118	0.056
5..	18.864	18.685	18.687	18.415	18.706	18.537	18.517	18.612	18.518	18.800	19.165	18.925
	0.085	0.079	0.077	0.082	0.085	0.086	0.089	0.091	0.101	0.114	0.161	0.155
6..	17.611	17.552	17.672	17.589	17.660	17.727	17.753	17.836	17.841	17.868	17.976	17.923
	0.030	0.029	0.028	0.031	0.032	0.039	0.038	0.044	0.046	0.064	0.108	0.062
7..	16.990	16.874	16.660	17.116	17.211	17.338	16.375	17.337	17.570	17.668	17.697	17.187
	0.019	0.018	0.013	0.022	0.023	0.029	0.014	0.030	0.038	0.054	0.085	0.033
8..	19.042	18.912	18.910	18.915	18.896	18.941	18.179	18.664	18.759	18.852	18.688	18.646
	0.083	0.083	0.083	0.083	0.078	0.081	0.075	0.076	0.079	0.083	0.094	0.088
9..	20.062	20.574	20.157	20.084	19.921	20.203	20.005	20.255	19.745	19.620	20.314	19.683
	0.106	0.108	0.098	0.094	0.098	0.104	0.099	0.114	0.115	0.130	0.182	0.160
10..	18.649	18.452	18.515	18.578	18.522	18.536	18.618	18.536	18.603	18.552	18.400	18.516
	0.066	0.056	0.051	0.066	0.062	0.074	0.073	0.074	0.082	0.114	0.156	0.100
11..	19.561	19.051	18.994	18.823	18.500	18.520	18.186	18.114	17.985	17.948	17.673	17.618
	0.153	0.098	0.080	0.085	0.063	0.075	0.052	0.053	0.050	0.067	0.081	0.046
12..	19.485	19.382	19.468	19.233	19.302	19.182	19.115	19.037	18.911	18.796	18.902	18.617
	0.092	0.091	0.092	0.091	0.096	0.094	0.101	0.100	0.105	0.098	0.111	0.107
13..	19.226	18.983	19.020	19.092	18.906	19.128	19.545	19.113	19.407	18.900	19.446	18.868
	0.106	0.087	0.077	0.101	0.084	0.121	0.165	0.120	0.165	0.146	0.380	0.131
14..	17.411	17.287	17.291	17.287	17.252	17.209	17.275	17.181	17.089	17.179	17.087	17.134
	0.024	0.022	0.019	0.023	0.021	0.023	0.024	0.023	0.023	0.032	0.045	0.029

Table 2: Continued

No.	03	04	05	06	07	08	09	10	11	12	13	14
(1)	(2)	(3)	(4)	(5)	(6)	(7)	(8)	(9)	(10)	(11)	(12)	(13)
19..	18.973	18.775	18.757	18.681	18.570	18.655	18.523	18.496	18.497	18.320	18.297	18.237
	0.088	0.074	0.063	0.072	0.065	0.083	0.068	0.072	0.076	0.093	0.143	0.079
20..	19.110	18.755	18.704	18.453	18.307	18.254	18.050	17.831	17.698	17.706	17.522	17.392
	0.102	0.077	0.063	0.063	0.054	0.061	0.048	0.043	0.040	0.055	0.072	0.038
21..	17.265	17.317	17.354	17.469	17.426	17.630	17.702	18.012	17.929	17.869	18.319	18.026
	0.023	0.024	0.021	0.029	0.025	0.035	0.036	0.050	0.049	0.060	0.139	0.065
22..	18.655	18.231	18.126	18.008	17.760	17.794	17.739	17.634	17.601	17.492	17.561	17.490
	0.065	0.046	0.037	0.040	0.032	0.038	0.035	0.034	0.035	0.043	0.071	0.040
23..	18.988	18.756	18.676	18.581	18.335	18.407	18.389	18.355	18.282	18.206	18.341	18.107
	0.085	0.071	0.057	0.065	0.051	0.064	0.059	0.062	0.062	0.079	0.139	0.067
24..	18.886	18.877	18.871	18.996	18.950	19.111	19.204	19.400	19.688	19.831	20.399	20.540
	0.081	0.082	0.071	0.097	0.093	0.127	0.129	0.166	0.228	0.372	0.990	0.654
25..	19.193	19.220	19.285	18.817	18.833	18.871	18.880	19.007	18.573	18.792	18.779	19.118
	0.079	0.068	0.073	0.061	0.071	0.074	0.079	0.072	0.070	0.092	0.188	0.145
26..	17.465	17.372	17.481	17.517	17.407	17.557	17.567	17.558	17.514	17.426	17.391	17.389
	0.029	0.028	0.027	0.035	0.028	0.038	0.038	0.040	0.041	0.045	0.063	0.041
27..	18.789	18.497	18.494	18.400	18.209	18.202	18.145	18.109	17.984	17.902	17.762	17.543
	0.088	0.071	0.061	0.072	0.055	0.064	0.059	0.062	0.059	0.065	0.083	0.045
28..	17.258	16.754	16.600	16.458	16.163	16.149	15.967	15.914	15.866	15.777	15.722	15.689
	0.024	0.017	0.013	0.014	0.010	0.012	0.010	0.010	0.010	0.011	0.015	0.010
29..	18.982	18.598	18.614	18.313	18.267	18.184	18.170	18.163	18.229	18.134	18.173	18.077
	0.056	0.049	0.043	0.041	0.036	0.038	0.039	0.043	0.052	0.051	0.055	0.062
30..	18.703	18.186	18.486	18.273	18.108	18.176	18.888	18.329	18.378	18.404	18.616	18.651
	0.070	0.046	0.052	0.053	0.043	0.053	0.101	0.062	0.069	0.093	0.173	0.108
31..	19.396	18.951	18.873	18.770	18.528	18.464	18.438	18.375	18.271	18.212	18.033	18.474
	0.129	0.089	0.071	0.081	0.064	0.071	0.065	0.067	0.065	0.083	0.109	0.097
32..	16.614	16.507	16.573	16.644	16.643	16.689	16.666	16.651	16.601	16.538	16.542	16.488
	0.015	0.014	0.012	0.016	0.015	0.017	0.016	0.017	0.017	0.021	0.031	0.018

Table 2: Continued

No.	03	04	05	06	07	08	09	10	11	12	13	14
(1)	(2)	(3)	(4)	(5)	(6)	(7)	(8)	(9)	(10)	(11)	(12)	(13)
36..	18.771	18.303	18.563	18.257	18.468	18.420	18.363	18.111	18.163	18.921	19.179	18.687
	0.071	0.048	0.051	0.048	0.057	0.064	0.056	0.048	0.054	0.154	0.308	0.112
37..	18.779	18.613	19.215	18.490	18.518	18.541	18.821	18.276	18.167	18.190	18.124	18.023
	0.079	0.069	0.110	0.065	0.067	0.079	0.112	0.063	0.061	0.087	0.128	0.070
38..	19.003	18.854	18.737	18.722	18.742	18.748	18.641	18.767	18.783	18.636	18.545	18.725
	0.093	0.083	0.064	0.079	0.079	0.094	0.080	0.096	0.104	0.126	0.181	0.126
40..	17.711	17.656	17.540	17.919	18.069	18.182	17.369	18.177	18.494	18.309	18.707	18.382
	0.024	0.023	0.019	0.028	0.031	0.038	0.020	0.039	0.046	0.068	0.120	0.063
43..	18.437	18.357	18.236	18.387	18.424	18.531	17.687	18.481	18.450	18.346	18.555	17.908
	0.044	0.041	0.034	0.034	0.035	0.034	0.018	0.038	0.032	0.035	0.052	0.032
44..	17.629	17.556	17.624	17.642	17.607	17.658	17.679	17.669	17.727	17.688	17.634	17.576
	0.030	0.029	0.026	0.032	0.030	0.037	0.035	0.038	0.042	0.054	0.079	0.045
45..	19.634	19.213	19.133	19.111	18.995	19.099	19.196	19.203	18.917	18.928	18.902	18.788
	0.150	0.105	0.084	0.102	0.089	0.115	0.119	0.128	0.104	0.145	0.222	0.118
46..	19.400	18.828	18.827	18.727	18.499	18.617	18.559	18.487	18.643	18.419	18.505	18.379
	0.133	0.082	0.071	0.080	0.063	0.082	0.074	0.074	0.090	0.101	0.169	0.090
47..	17.547	17.357	17.414	17.382	17.214	17.227	17.183	17.165	17.209	17.296	17.288	17.159
	0.025	0.023	0.021	0.025	0.023	0.027	0.023	0.025	0.027	0.039	0.059	0.032
48..	18.878	18.853	18.967	18.862	18.691	18.790	19.521	18.639	18.805	18.790	18.593	18.692
	0.088	0.089	0.084	0.095	0.075	0.096	0.185	0.087	0.108	0.136	0.172	0.118
49..	19.374	18.537	18.556	18.518	18.081	18.068	17.862	17.905	17.928	17.743	17.797	17.810
	0.151	0.073	0.065	0.078	0.049	0.057	0.046	0.050	0.054	0.059	0.094	0.059
50..	18.633	18.272	18.249	18.411	18.227	18.282	18.205	18.457	18.367	18.246	18.172	18.094
	0.065	0.049	0.041	0.059	0.048	0.059	0.052	0.071	0.069	0.083	0.120	0.067
51..	18.626	18.513	18.554	18.519	18.446	18.375	18.508	18.317	18.475	18.506	18.553	19.044
	0.080	0.073	0.077	0.093	0.102	0.098	0.092	0.100	0.082	0.109	0.176	0.081
52..	19.742	19.233	19.102	19.202	18.741	18.901	18.707	18.744	18.805	18.592	18.570	18.688
	0.161	0.104	0.080	0.109	0.072	0.098	0.077	0.086	0.096	0.111	0.170	0.111

Table 2: Continued

No.	03	04	05	06	07	08	09	10	11	12	13	14
(1)	(2)	(3)	(4)	(5)	(6)	(7)	(8)	(9)	(10)	(11)	(12)	(13)
56..	18.662	18.454	18.469	18.414	18.308	18.342	18.362	18.343	18.471	18.437	18.508	18.196
	0.068	0.058	0.051	0.060	0.054	0.065	0.061	0.065	0.078	0.105	0.175	0.078
57..	19.939	19.766	19.506	19.471	18.933	19.041	18.786	18.848	18.532	18.321	18.256	18.157
	0.206	0.177	0.120	0.144	0.091	0.118	0.086	0.099	0.080	0.095	0.142	0.075
58..	18.762	18.537	18.585	18.546	18.387	18.478	18.388	18.534	18.572	18.430	18.127	18.359
	0.074	0.061	0.055	0.065	0.057	0.072	0.061	0.076	0.083	0.105	0.126	0.090
59..	18.467	18.294	18.284	18.194	17.923	17.976	17.872	17.689	17.484	17.382	17.338	17.155
	0.046	0.038	0.034	0.037	0.033	0.036	0.031	0.029	0.026	0.034	0.050	0.028
60..	18.798	18.714	18.664	18.648	18.676	18.703	18.689	18.783	18.806	18.713	19.077	18.649
	0.074	0.070	0.057	0.068	0.071	0.085	0.077	0.091	0.099	0.131	0.291	0.113

Table 3: Comparison of Cluster Photometry with Previous Measurements

No.	V (Chandar et al.)	V (BATC)	$B - V$ (Chandar et al.)	$B - V$ (BATC)
(1)	(2)	(3)	(4)	(5)
1.....	18.594 ± 0.018	18.722 ± 0.148	0.028 ± 0.020	-0.005 ± 0.275
2.....	16.756 ± 0.006	16.696 ± 0.032	0.214 ± 0.006	-0.015 ± 0.060
3.....	17.416 ± 0.010	17.674 ± 0.054	0.294 ± 0.023	-0.062 ± 0.097
4.....	17.851 ± 0.006	17.888 ± 0.063	0.176 ± 0.011	0.008 ± 0.114
5.....	18.621 ± 0.013	18.726 ± 0.139	0.068 ± 0.019	0.073 ± 0.254
6.....	17.862 ± 0.008	17.674 ± 0.054	-0.186 ± 0.013	-0.062 ± 0.097
7.....	17.384 ± 0.006	17.198 ± 0.039	-0.131 ± 0.006	-0.224 ± 0.069
8.....	18.856 ± 0.019	18.947 ± 0.131	0.352 ± 0.030	0.069 ± 0.250
9.....	19.670 ± 0.032	19.942 ± 0.161		0.686 ± 0.314
10.....	18.774 ± 0.016	18.595 ± 0.108		-0.039 ± 0.190
11.....	18.808 ± 0.016	18.657 ± 0.115		0.594 ± 0.265
12.....	19.008 ± 0.021	19.377 ± 0.155	0.297 ± 0.034	0.082 ± 0.288
13.....	18.667 ± 0.019	18.953 ± 0.156	0.208 ± 0.016	0.149 ± 0.283
14.....	17.339 ± 0.005	17.336 ± 0.036	0.170 ± 0.008	0.051 ± 0.067
15.....	19.008 ± 0.023	19.058 ± 0.159	0.409 ± 0.028	0.340 ± 0.316
16.....	17.449 ± 0.005	17.271 ± 0.036	0.267 ± 0.009	-0.039 ± 0.064
18.....	19.870 ± 0.046	19.666 ± 0.250	0.007 ± 0.038	-0.004 ± 0.437
19.....	18.752 ± 0.016	18.637 ± 0.116		0.260 ± 0.223
20.....	18.302 ± 0.005	18.430 ± 0.094		0.489 ± 0.208
21.....	17.713 ± 0.008	17.433 ± 0.046	-0.190 ± 0.008	-0.062 ± 0.080
22.....	17.935 ± 0.007	17.888 ± 0.058	0.513 ± 0.016	0.534 ± 0.126
23.....	18.264 ± 0.010	18.450 ± 0.093	0.548 ± 0.017	0.449 ± 0.195
24.....	18.904 ± 0.017	18.972 ± 0.166	-0.044 ± 0.016	-0.017 ± 0.281
25.....	18.840 ± 0.018	18.875 ± 0.114	0.692 ± 0.039	0.399 ± 0.216
26.....	17.535 ± 0.022	17.453 ± 0.052	0.172 ± 0.027	-0.011 ± 0.093
27.....	18.077 ± 0.022	18.332 ± 0.098	0.273 ± 0.035	0.305 ± 0.203
28.....	16.368 ± 0.015	16.322 ± 0.019	0.794 ± 0.014	0.652 ± 0.044
29.....	18.437 ± 0.035	18.368 ± 0.062	0.985 ± 0.059	0.386 ± 0.133
30.....	18.124 ± 0.041	18.198 ± 0.077	0.273 ± 0.037	0.110 ± 0.150
31.....	18.508 ± 0.031	18.686 ± 0.113	0.428 ± 0.040	0.455 ± 0.247
32.....	16.703 ± 0.016	16.687 ± 0.025	0.079 ± 0.013	-0.097 ± 0.045

Table 3: Continued

No.	V (Chandar et al.)	V (BATC)	$B - V$ (Chandar et al.)	$B - V$ (BATC)
(1)	(2)	(3)	(4)	(5)
33.....	17.141 ± 0.020	17.141 ± 0.031	0.218 ± 0.018	0.118 ± 0.060
34.....	17.722 ± 0.021	17.641 ± 0.051	0.137 ± 0.020	0.005 ± 0.094
35.....	17.145 ± 0.017	17.135 ± 0.031	0.150 ± 0.015	0.012 ± 0.056
36.....	18.553 ± 0.034	18.474 ± 0.093	0.222 ± 0.033	-0.051 ± 0.168
37.....	18.636 ± 0.033	18.561 ± 0.113	0.244 ± 0.033	0.163 ± 0.230
38.....	18.655 ± 0.032	18.793 ± 0.135	0.202 ± 0.040	0.195 ± 0.253
40.....	18.505 ± 0.010	18.043 ± 0.052	-0.338 ± 0.010	-0.301 ± 0.125
43.....	18.575 ± 0.018	18.436 ± 0.057	0.755 ± 0.039	0.012 ± 0.115
44.....	17.735 ± 0.007	17.661 ± 0.052	0.288 ± 0.009	-0.030 ± 0.093
45.....	19.074 ± 0.024	19.058 ± 0.159	0.535 ± 0.026	0.340 ± 0.316
46.....	18.474 ± 0.013	18.594 ± 0.116	0.764 ± 0.017	0.436 ± 0.243
47.....	17.264 ± 0.005	17.323 ± 0.040	0.497 ± 0.007	0.137 ± 0.072
48.....	18.794 ± 0.100	18.773 ± 0.137	0.417 ± 0.026	0.134 ± 0.264
49.....	18.079 ± 0.011	18.285 ± 0.092	0.824 ± 0.017	0.507 ± 0.213
50.....	18.132 ± 0.006	18.328 ± 0.087	0.360 ± 0.014	0.104 ± 0.159
51.....	18.838 ± 0.022	18.552 ± 0.164	0.459 ± 0.026	0.052 ± 0.272
52.....	18.618 ± 0.016	18.897 ± 0.139	0.810 ± 0.027	0.552 ± 0.296
53.....	19.563 ± 0.027	19.359 ± 0.187		0.583 ± 0.434
54.....	18.407 ± 0.010	18.383 ± 0.076	1.075 ± 0.020	0.598 ± 0.176
55.....	18.104 ± 0.006	18.112 ± 0.068		0.295 ± 0.135
56.....	18.408 ± 0.008	18.390 ± 0.094		0.181 ± 0.178
57.....	19.375 ± 0.015	19.131 ± 0.176		0.805 ± 0.425
58.....	18.391 ± 0.006	18.468 ± 0.101		0.182 ± 0.190
59.....	18.649 ± 0.009	18.052 ± 0.056		0.356 ± 0.112
60.....	18.679 ± 0.008	18.717 ± 0.121		0.101 ± 0.220

Table 4: Age and Metallicity Distribution of 56 Star Clusters

No.	Metallicity (Z)	Age ([log yr])	No.	Metallicity (Z)	Age ([log yr])
(1)	(2)	(3)	(1)	(2)	(3)
1.....	0.02000	7.260	30.....	0.00400	6.620
2.....	0.05000	6.860	31.....	0.00040	9.207
3.....	0.00400	6.620	32.....	0.02000	6.880
4.....	0.00040	8.009	33.....	0.00400	8.009
5.....	0.00040	8.009	34.....	0.00040	7.806
6.....	0.00400	6.820	35.....	0.00040	7.806
7.....	0.00400	6.439	36.....	0.00040	7.806
8.....	0.00040	6.620	37.....	0.02000	6.940
9.....	0.02000	7.477	38.....	0.02000	8.255
10.....	0.00400	7.320	40.....	0.00400	6.420
11.....	0.00400	10.301	43.....	0.02000	7.121
12.....	0.02000	6.940	44.....	0.00400	7.220
13.....	0.00040	7.806	45.....	0.00040	8.009
14.....	0.00400	6.980	46.....	0.00040	8.957
15.....	0.00400	8.009	47.....	0.02000	8.057
16.....	0.00400	7.079	48.....	0.00040	8.009
18.....	0.02000	7.279	49.....	0.00040	9.342
19.....	0.00400	6.940	50.....	0.02000	8.057
20.....	0.02000	9.544	51.....	0.00040	7.806
21.....	0.02000	6.580	52.....	0.00040	9.107
22.....	0.00040	9.255	53.....	0.00400	8.957
23.....	0.00040	8.957	54.....	0.00040	9.009
24.....	0.02000	6.520	55.....	0.00040	8.957
25.....	0.00400	8.009	56.....	0.00040	8.009
26.....	0.00400	7.241	57.....	0.00400	10.279
27.....	0.02000	8.857	58.....	0.00400	6.960
28.....	0.00040	9.796	59.....	0.02000	9.107
29.....	0.00400	8.009	60.....	0.00040	7.806

Table 5: Metallicity, Reddening and Age Distribution of 7 Star Clusters

No.	Metallicity (Z)	$E(B - V)$	Age ($[\log \text{yr}]$)
11.....	0.00099	0.200	10.30
20.....	0.00719	0.110	10.30
22.....	0.00186	0.140	9.23
28.....	0.00023	0.050	10.30
49.....	0.00040	0.010	9.92
54.....	0.00890	0.010	9.40
59.....	0.01447	0.010	10.28

This figure "majunfig1.gif" is available in "gif" format from:

<http://arXiv.org/ps/astro-ph/0106487v1>